

ALD-ZnMgO and absorber surface modifications to substitute CdS buffer layers in co-evaporated CIGSe solar cells

Ramis Hertwig*, Shiro Nishiwaki, Mario Ochoa, Shih-Chi Yang, Thomas Feurer, Evgeniia Gilshtein, Ayodhya N. Tiwari, and Romain Carron

Laboratory for Thin Films and Photovoltaics, Empa-Swiss Federal Laboratories for Materials Science and Technology, Ueberlandstrasse 129, 8600 Duebendorf, Switzerland

Received: 15 July 2020 / Received in final form: 24 September 2020 / Accepted: 8 December 2020

Abstract. High efficiency chalcopyrite thin film solar cells generally use chemical bath deposited CdS as buffer layer. The transition to Cd-free buffer layers, ideally by dry deposition methods is required to decrease Cd waste, enable all vacuum processing and circumvent optical parasitic absorption losses. In this study, $Zn_{1-x}Mg_xO$ thin films were deposited by atomic layer deposition (ALD) as buffer layers on co-evaporated $Cu(In,Ga)Se_2$ (CIGS) absorbers. A specific composition range was identified for a suitable conduction band alignment with the absorber surface. We elucidate the critical role of the CIGS surface preparation prior to the dry ALD process. Wet chemical surface treatments with potassium cyanide, ammonium hydroxide and thiourea prior to buffer layer deposition improved the device performances. Additional in-situ surface reducing treatments conducted immediately prior to $Zn_{1-x}Mg_xO$ deposition improved device performance and reproducibility. Devices were characterised by (temperature dependant) current-voltage and quantum efficiency measurements with and without light soaking treatment. The highest efficiency was measured to be 18%.

Keywords: Thin film solar cells / $Cu(In,Ga)Se_2$ buffer / ZnMgO / ALD / surface treatment

1 Introduction

Prior to the recent record cells [1], the best performing thin film solar cells with chalcopyrite absorbers ($Cu(In,Ga)(S,Se)_2$) have employed chemical bath deposited (CBD) CdS as the buffer layer [2–4] over alternative buffer materials or deposition methods [5–7]. CdS shows best performances when bath deposited, and is an inherently limiting material for a buffer layer due to its low band gap (E_g) of 2.4 eV [8] and the associated parasitic absorption. Therefore, industrial manufacturing is hindered by the added complexity of a highly uniform wet deposition step between vacuum deposition steps, the low material yield and the Cd-contaminated waste treatment. The ability to tailor the buffer layer to the absorber in terms of band alignment, transparency or lattice mismatch are increasingly necessary when absorber modifications such as alkali post deposition treatment (PDT) [2,9] or Ag incorporation affect the surface [10–12]. High E_g materials like oxides, sulfides and selenides of In and Zn are recognized as the most promising material choices, as suggested in reviews discussing the difficulties of substituting CBD-CdS with alternative materials or deposition methods [13–15]. The recent improvements on alternatives to CdS, namely

CBD-Zn(O,S) [1] and notably the $Zn_{1-x}Mg_xO$ deposited by dry sputtering method [16], surpass the CBD-CdS buffer layer in terms of device efficiency, which was attributed to increased current, bespoke interface engineering and the consequential reduction of recombination [17].

$Zn_{1-x}Mg_xO$ is suited as buffer material due to its tuneable bandgap (3.2 eV for i-ZnO, 3.8 eV for $Zn_{0.8}Mg_{0.2}O$, 7.7 eV for MgO [18,19]), and the accompanied change of the conduction band minimum (CBM) position from below the CBM of CIS (i-ZnO) to clearly higher than CGS [20,21]. $Zn_{1-x}Mg_xO$ has been shown to be a viable buffer in case the conduction band offset (CBO) with the absorber is within 0–0.3 eV [22,23]. $Zn_{1-x}Mg_xO$ has been implemented as buffer layer in CIGS devices with efficiencies higher than 15% by sputtering [16,24] or atomic layer deposition (ALD) [25–28]. Sputter deposition directly on the absorber is reported to cause sputter damage [29,30], leading to defective interfaces and V_{OC} losses due to interface recombination [31,32]. This can be mitigated by introducing a thin intermediate layer, or using a soft deposition method, for example ALD or indirect sputtering [16].

Devices with alternative buffer layers are prone to metastabilities [33–36], which can improve the performance after exposure to light, elevated temperatures or a combination of both [37,38]. The precise nature of metastable enhancement is still debated and may differ

* e-mail: ramis.hertwig@empa.ch

depending on the processing methods and materials of devices. The possible causes include presence of detrimental negative charges, for example associated with hydrogen or oxygen [34,37], which become inactive after hole capture holes upon light exposure. Another possibility is an interplay between vacancy complexes at the absorber and the buffer [35,39,40].

This work focuses on the substitution of CBD-CdS with a dry deposited high bandgap material and the effects of surface modifications before the growth of the buffer layer. The approach to prepare the absorber surface is inspired by the chemical environment in a typical CdS-CBD solution prior to CdS growth. First, the properties of the ALD deposited $\text{Zn}_{1-x}\text{Mg}_x\text{O}$ thin films are analysed in terms of thickness, composition, carrier density, mobility and sheet resistance. This high E_g material allows modification of the conduction band minimum [41,42] in the vicinity of the ones of CIS and CGS [21], which is used to match the conduction band of the absorber. The variation of the Mg content of the device performance will be discussed. We investigate the influence of different absorber surface treatments before $\text{Zn}_{1-x}\text{Mg}_x\text{O}$ deposition on the final device properties, notably KCN, ammonia and variants inspired by the successful CdS-CBD deposition process. Absorber dry treatments with trimethylaluminium (TMA) performed in the ALD chamber are also investigated. The effects of wet and dry absorber treatments before the buffer deposition are discussed and resulting cells are compared to CdS-CBD references.

2 Experimental

CIGS absorbers were grown on molybdenum-coated soda lime glass by a multistage co-evaporation process at about 450 °C and were subject to NaF and RbF PDT treatment. The growth process is described in [43]. The integrated ratio of Cu to In+Ga (CGI) and Ga to In+Ga (GGI) is 0.96 and 0.40, respectively, with the GGI near the surface being about 0.3. Typical gradings can be found in [43,44]. As standard treatment, the absorbers were etched in 10%_w potassium cyanide (KCN) for 3 min, and in NH_4OH (2 M $[\text{NH}_3]$) aqueous solution for 1 min with H_2O rinsing after each step. The transfer time between absorber surface treatments and ALD vacuum was less than 5 min. ZnMgO was deposited by ALD in a Fiji G2 system (Ultratech). Diethylzinc (DEZ), bis(cyclopentadienyl)magnesium (MgCp_2), trimethylaluminium (TMA) and H_2O (0.06 s) precursors were used at 120 °C substrate temperature, with Ar carrier gas at a base pressure of 13 Pa. Growth cycles are $\text{ZnO} = \text{H}_2\text{O}/\text{N}_2/\text{DEZ}/\text{N}_2 = 0.06/17/0.1/5$ s, $\text{MgO} = \text{H}_2\text{O}/\text{N}_2/\text{MgCp}_2/\text{N}_2 = 0.06/17/2/5$ s, $\text{Al}_2\text{O}_3 = \text{H}_2\text{O}/\text{N}_2/\text{TMA}/\text{N}_2 = 0.06/17/0.06/10$ s for ZnO, MgO and Al_2O_3 , respectively. MgCp_2 was heated to 90 °C, the other precursors were kept at room temperature. The stoichiometry of ZnMgO was varied by the relative numbers of DEZ to MgCp_2 pulses, for example a ratio of 9 cycles DEZ/ H_2O followed by one cycle of $\text{MgCp}_2/\text{H}_2\text{O}$ were used for $\text{Zn}_{0.9}\text{Mg}_{0.1}\text{O}$. $\text{Zn}_{1-x}\text{Mg}_x\text{O}$ thin films were simultaneously deposited on CIGS absorbers, Si (100) and soda-lime glass substrates. Targeted buffer thickness is 28 nm. A similar

thickness is used for the CBD-CdS reference sample, which was performed using 185 ml H_2O , 35 ml NH_4OH , 15 ml Cd-acetate and 15 ml thiourea (TU) for 14 min at 70 °C. Where specified in the manuscript, solutions containing not all but the same ratio of ingredients as the CdS-CBD were used for surface treatments. The devices are finished with rf-magnetron sputtered ZnO (70 nm) and ZnO:Al (200 nm) layers in an Ar/ O_2 atmosphere at a pressure of 0.46 Pa and a power density of 1 and 2.5 W cm^{-2} , respectively. Ni/Al grid contacts are e-beam deposited (50 nm, 4000 nm). The cell area is defined by mechanical scribing and determined from scans on a flatbed scanner. The cell area for the reference device is 0.512 cm^2 , for the $\text{Zn}_{1-x}\text{Mg}_x\text{O}$ buffer devices the area varies around 0.2 cm^2 .

The ALD buffer layer composition was analysed by X-ray photoelectron spectroscopy (XPS) using a Quantum 2000 photoelectron spectrometer from Physical Electronics with a monochromatic Al $K\alpha$ source, operated at a base pressure below 10^{-9} mbar. The detailed high-resolution Mg 2p peak at 51 eV and Zn 2p peaks at 1022 eV with spin-orbit components splitting of 23 eV were acquired after 10 s of surface sputtering cycle. Peak spectra were recorded with an energy step size of 0.125 eV and a pass energy of 29.35 eV. An ion neutralizer using Ar^+ of ≈ 1 eV was used to minimize the fluctuations of the binding energy values. The instrument work function was calibrated to give an Au $4f_{7/2}$ metallic gold binding energy of 84 eV. The acquired data were analyzed using PHI MultiPak software. Quantitative analysis was performed by measuring the Mg 2p and Zn 2p peak areas and by applying appropriate relative sensitivity factors (4.431 and 85.057).

The $\text{Zn}_{1-x}\text{Mg}_x\text{O}$ layer thickness was determined by ellipsometry on a M-2000 device using Si(100) substrates. Hall measurements were performed using a ECOPIA HMS3000 apparatus with 4 contacts in van der Pauw configuration. I-V characterisation was carried out with a Keithley 2400 source meter and four-terminal contacting under standard test conditions (1000 W m^{-2} , 298 K) using an ABA type solar simulator on relaxed samples unless stated otherwise. Temperature dependent electrical measurements (TIV and J_{SC} vs V_{OC}) were performed in a cryostat cooled with liquid nitrogen with illumination provided by a halogen lamp with variable intensity filters. External quantum efficiency (EQE) characterisation was performed with a chopped halogen light source, a triple-grating monochromator and a lock-in amplifier at 298 K. A certified monocrystalline Si solar cell was used as reference device for both, EQE and I-V measurements.

3 Results and discussion

3.1 ZnMgO thin film

$\text{Zn}_{1-x}\text{Mg}_x\text{O}$ thin films were deposited on Si (100) and soda-lime glass substrates simultaneously with the deposition on CIGS absorbers. The nominal Mg content (ratio of $\frac{\text{Mg}}{\text{Zn}+\text{Mg}}$ pulses) is approximated from the ratio of Zn and Mg pulses, disregarding the intricacies of the ALD deposition process. The Mg content of deposited layers was varied between 5%

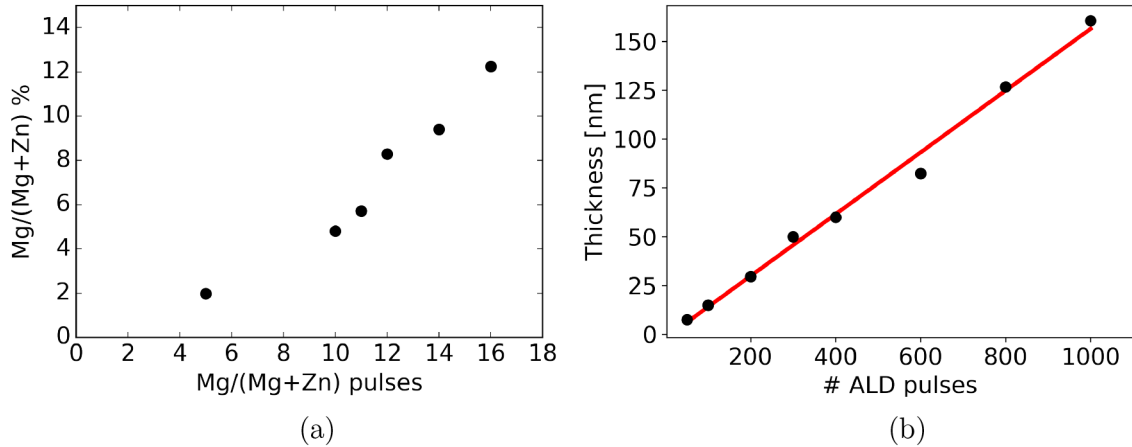


Fig. 1. (a) Mg/(Zn+Mg) content in Zn_{1-x}Mg_xO films as determined by XPS as function of the nominal value based on the number of pulses. (b) Zn_{1-x}Mg_xO film thickness with number of deposition pulses as determined by ellipsometry. A linear fit (line) results in layer growth of 1.65 Å per pulse.

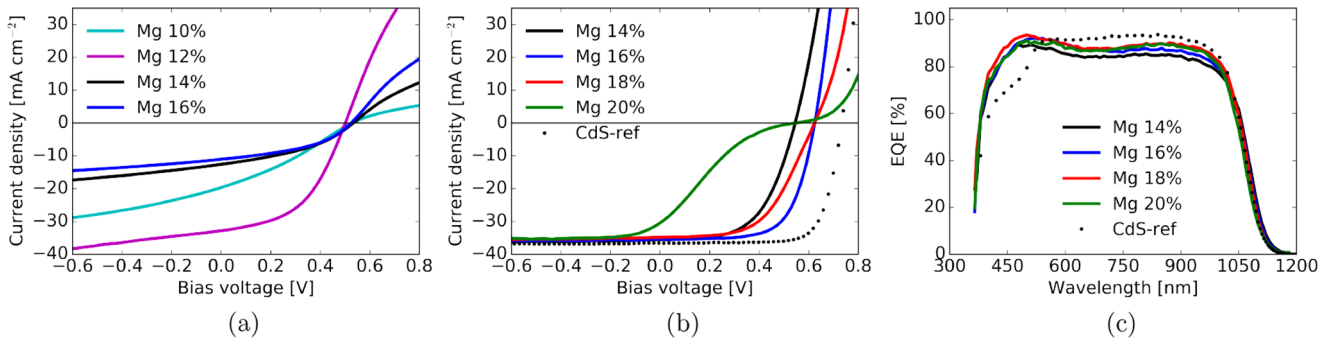


Fig. 2. (a) IV curves of samples treated with KCN only before buffer deposition. (b) IV curves of samples subjected to KCN and NH₄OH treatment. (c) EQE of samples with absorbers treated with KCN and NH₄OH.

and 16% by adjusting the ratio of Zn and Mg pulse numbers, and then analysed by XPS. As shown in Figure 1a, the Mg content determined using XPS does follow the nominal trend, similar to [25,28]. Zn_{1-x}Mg_xO layers with Mg content of 16% deposited on Si substrates show linear growth of 1.65 Å per cycle between 50 and 1000 combined Zn and Mg cycles as determined by ellipsometry on Si(100) wafers, as visible in Figure 1b. Hall measurements could only be acquired with the thickest deposited layer (1000 cycles, 160 nm), resulting in a carrier density of $2.7 \times 10^{19}/\text{cm}^3$, a mobility of $1.8 \text{ cm}^2/\text{Vs}$ and a sheet resistance of $4.96 \times 10^3 \Omega/\text{sq}$, measured on soda lime glass.

3.2 Influence of Mg content on device performance

A conduction band offset of 0–0.3 eV with respect to CIGS [23,45] is targeted by adjusting the Mg content in the Zn_{1-x}Mg_xO buffer layer. The CBM of ZnO is reported equal to that of CIS, whereas the CBM of CuGaSe₂ is 0.6–0.7 eV higher [21]. The addition of Mg in ZnO increases the CBM and lowers the VBM, which has been shown to

result in a better alignment [22,25,46]. Considering the band gap variation from ZnO to Zn_{0.8}Mg_{0.2}O is reported to be 0.6 eV [19], a range of 10% nominal Mg content variations is expected to have little influence on device performance. The targeted buffer thickness is 28 nm, which is comparable to the thickness of the CBD-CdS buffer layer. The thickness of the Zn_{1-x}Mg_xO buffer layer does affect the device performance, but since this can be attributed to an interplay of the buffer with the window layers, this effect is not discussed here [38].

The first absorber series was only rinsed in KCN before buffer deposition. This treatment cleans the absorber and removes alkali species from the surface as reported in [47]. As depicted in Figure 2a, all devices exhibit poor PV performance for Mg content between 10% and 20%, and the V_{OC} is between 500 and 530 mV. There is no obvious correlation of the PV parameters with the content of Mg in the buffer layer, see Table 1. As CBD-CdS has been successfully applied to a variety of different absorbers, the hypothesis has been made that the absorber surface is beneficially modified during the initial stages of the

Table 1. PV parameters of devices with KCN only surface treatment, see Figure 2a. Percentages correspond to the Mg content of the buffer layer.

$2 \times \frac{Mg}{Zn+Mg}$	V_{OC} (mV)	J_{SC} (mA/cm ²)	FF (%)	η (%)
10%	528	19.6	30	3.2
12%	501	32.8	48	8.0
14%	533	12.6	39	2.6
16%	525	11.0	43	2.5

Table 2. PV parameters of devices with KCN and NH₄OH surface treatment, see Figure 2b. Percentages correspond to the Mg content of the buffer layer.

$2 \times \frac{Mg}{Zn+Mg}$	V_{OC} (mV)	J_{SC} (mA/cm ²)	FF (%)	η (%)
14%	545	35.6	57	11.0
16%	624	35.5	67	14.7
18%	623	34.8	55	12.0
20%	547	30.2	17	3.0

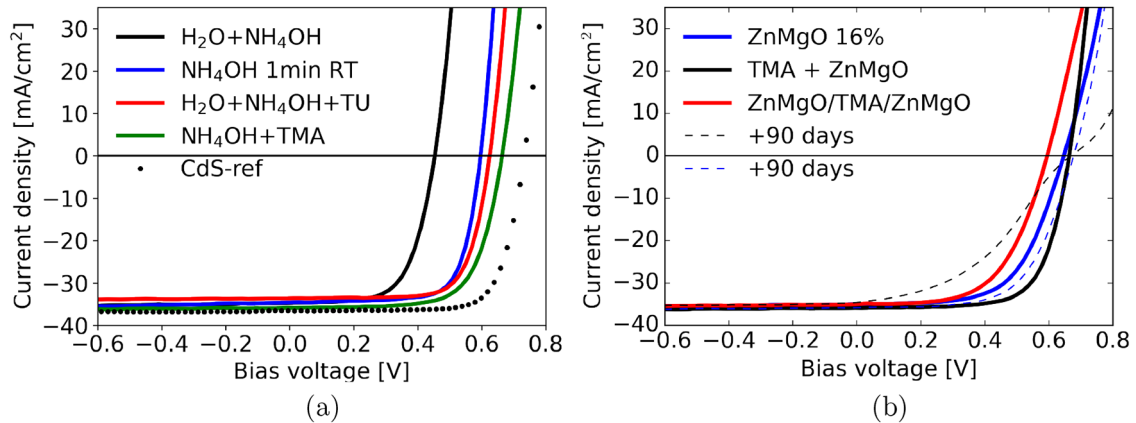


Fig. 3. (a) Effect of wet treatment before buffer deposition on JV curves. Absorber treatments with NH₄OH or thiourea-ammonia solution show increased V_{OC} . Additional (b) Influence of a single TMA pulse before and during buffer deposition, with unchanged total ZnMgO thickness. TMA before Zn_{1-x}Mg_xO increases V_{OC} and reduces ageing. TMA during Zn_{1-x}Mg_xO reduces V_{OC} .

deposition process [48,49]. This leads to the assumption, that a surface modification of the absorber which takes place during the initial stages of CdS-CBD is missing.

The following analysis investigates the effect of a treatment in a solution containing some, but not all ingredients of the CdS-CBD solution in the same ratio, for example, H₂O, NH₄OH and TU. After being cleaned in KCN and rinsed with H₂O, the absorbers were immersed in NH₄OH for 1 min. As shown in Figure 2b, a clear improvement in V_{OC} and FF is observed for Zn_{1-x}Mg_xO buffer layers with Mg content from 14% to 20%, with 16% Mg resulting in the best device performance, listed in Table 2. Devices with lower Mg content in the buffer layer exhibit lower V_{OC} , while higher Mg content show a loss in FF, similarly as reported in [23,25,45,50]. This can be attributed to the formation of a cliff-like band alignment for low Mg content, which increases recombination and therefore reduces V_{OC} . High Mg content raises the CB of the buffer layer to form a spike-like conduction band offset, which results in a blocking of photocurrent. It should be noted that variations in nominal Mg content of 2% already show drastic variations in device performance, narrower than the expected process window of about 10% nominal Mg content. In analogy to [51], a non-uniform composition over the very first monolayers could be speculated, which could lead to the formation of a blocking barrier.

The performance of the devices is not as good as the CdS reference, which is mostly due to the lower V_{OC} and FF. The small deficit in J_{SC} is attributed to reflection losses arising from non optimised layer thicknesses and comparatively larger grid shading. Analysis of the EQE curves reveals a potential for J_{SC} gain arising from the wider buffer bandgap of about 1.1 mA/cm² in the range of 360–550 nm (see Fig. 2c). The absorber bandgap extracted from EQE using Tauc fit procedure is 1.14 eV. The following sections will focus on the improvements of V_{OC} and FF for buffer layers with 16% Mg content.

3.3 Absorber surface treatments

As shown before, samples treated with KCN and NH₄OH show an increase in V_{OC} and FF compared to samples which were etched only with KCN. The improvement can be attributed to a beneficial surface modification during the NH₄OH treatment. To investigate the analogies of KCN and NH₄OH surface treatments with the surface modifications during CdS-CBD, wet treatments of 1 min have been conducted with solutions resembling parts of the CdS-CBD process. The solutions used are H₂O + NH₄OH, NH₄OH, H₂O + NH₄OH + TU. Devices that have been treated with H₂O + NH₄OH show a reduction in V_{OC} with 453 mV (FF 64%), see Figure 3a. The absorber treated with

Table 3. PV parameters of devices with KCN and CBD-CdS alike surface treatment, see [Figures 3a](#) and [3b](#). All devices have buffer layers of ALD deposited $\text{Zn}_{0.8}\text{Mg}_{0.16}\text{O}$, 28 nm.

$2 \times \frac{\text{Mg}}{\text{Zn}+\text{Mg}}$	V_{OC} (mV)	J_{SC} (mA/cm ²)	FF (%)	η (%)
H ₂ O + NH ₄ OH	453	34.7	64	10.0
NH ₄ OH	596	34.6	73	15.1
H ₂ O + NH ₄ OH + TU	625	33.61	73	15.3
NH ₄ OH + TMA	663	35.9	69	16.5

28% NH₄OH solution shows a significantly increased V_{OC} of 597 mV (FF 73%). Solutions containing TU and NH₄OH result in increases in V_{OC} to 625 mV (FF 73%) over pure NH₄OH, which is tentatively attributed to S incorporation and the consequential higher carrier density of the absorber surface and shorter depletion region as reported in [52–54].

Even with TU and NH₄OH treatments, the best achieved V_{OC} and FF are significantly lower than the CdS reference sample, as reported in [Table 3](#). To further treat the absorber surface, TMA was pulsed once in the ALD chamber before buffer deposition. The resulting V_{OC} of 664 mV (FF 69%) yield a device efficiency of 16.5% without light and or heat soaking, as listed in [Table 4](#). No further change in device performance was observed when repeating TMA pulses prior to $\text{Zn}_{1-x}\text{Mg}_x\text{O}$ deposition, similarly as reported in [55]. Hence, the improvement by a single pulse of TMA can be attributed to further etching of the absorber surface, formation of local Al₂O₃ islands with passivating effect, or a chemical reduction of surface species [56]. Another possibility which needs to be addressed is the potential doping of $\text{Zn}_{1-x}\text{Mg}_x\text{O}$ with Al and the corresponding change in carrier density [57]. The improvement in V_{OC} is unlikely the result of a further increase in the CBM. ZnMgO:Al has a higher CB and lower VB than ZnMgO, hence it can be seen as a strong substitute for Mg. The introduction of Al will change the composition relative to the pulse ratio, which is one pulse of Al in 198 total pulses or roughly 0.5%. This would represent a ZnMgO:Al which is expected to behave like a ZnMgO with more than 16% Mg content, which are shown to have lower FF and not higher V_{OC} , see [Figure 3b](#). For comparison, TMA was also pulsed halfway through the $\text{Zn}_{1-x}\text{Mg}_x\text{O}$ deposition and directly compared to a device where TMA was pulsed at the very beginning, see [Figure 3b](#). If Al distributes evenly in $\text{Zn}_{1-x}\text{Mg}_x\text{O}$ as reported in [58], the expected outcome would be the same. The device where TMA is pulsed in the middle of the buffer deposition exhibits a lower V_{OC} and FF, which indicates absorber surface treatment instead of modification of the buffer layer. In case the single TMA pulse during the buffer deposition creates a uniform blocking layer, the charge carriers are able to tunnel through. The improvement of pulsing TMA at the beginning of the buffer deposition are primary in FF (61–69%) and secondary in V_{OC} (647–664 eV), which support the hypothesis of a surface treatment further. In addition, the beneficial effect of TMA extends to a reduction in aging of the device. Devices without TMA

Table 4. PV parameters of best devices with single TMA pulse during buffer deposition. “B” refers to a single cycle of TMA before buffer deposition, “M” refers to a single TMA pulse midway during buffer deposition.

$2 \times \frac{\text{Mg}}{\text{Zn}+\text{Mg}}$	V_{OC} (mV)	J_{SC} (mA/cm ²)	FF (%)	η (%)
B	663	35.9	69	16.5
B (+90 days)	677	35.8	62	15.0
M	594	35.0	58	12.2
M (+90 days)	668	34.5	42	9.6

Table 5. PV parameters of best performing device before and after light soaking at 1 sun, measured 90 days after finishing the cell.

Duration	V_{OC} (mV)	J_{SC} (mA/cm ²)	FF (%)	η (%)
–90 days	663	35.9	69	16.5
0 min	677	35.8	62	15.0
2 min	679	35.9	65	15.9
45 min	689	35.9	70	17.5
390 min	693	35.9	72	18.0

display a loss in FF from 61% to 41% over 3 months storage in ambient conditions, as compared to 69–62% with TMA ([Tab. 5](#)).

3.4 Metastabilites and interface recombination

The presented devices with $\text{Zn}_{1-x}\text{Mg}_x\text{O}$ buffer show a reversible light soaking effect. The evolution of the IV curve for the best performing device with $\text{Zn}_{1-x}\text{Mg}_x\text{O}$ buffer device is presented in [Figure 4a](#). The FF increases from 61% to 65% already after 2 min (1 sun illumination). Light exposure of 45 min increases the FF to 71%, accompanied by an increase in V_{OC} from 679 to 689 mV, resulting in 17.5% efficiency. Further light soaking up to 390 min improves FF to 72%, V_{OC} 693 mV and 18% efficiency. Similar effects have been reported by others for $\text{Zn}_{1-x}\text{Mg}_x\text{O}$ and other materials [28,32,59] ([Fig. 4](#)).

Different mechanisms can decrease the V_{OC} , for example increased interface recombination, reduction in carrier lifetimes at the interface [60,61], change in doping level of the absorber surface due to inter-diffusion [26,48], or photocurrent blocking barriers [32,59]. We can exclude inappropriate conduction band offsets as the Mg content in the buffer layer was systematically investigated (see [Sect. 3.2](#)).

In order to assess the interface quality, the best $\text{Zn}_{1-x}\text{Mg}_x\text{O}$ buffer device and the corresponding CdS reference device have been analysed with temperature dependant $J_{\text{SC}} - V_{\text{OC}}$ measurements at different light intensities. The $\text{Zn}_{1-x}\text{Mg}_x\text{O}$ buffer device has been

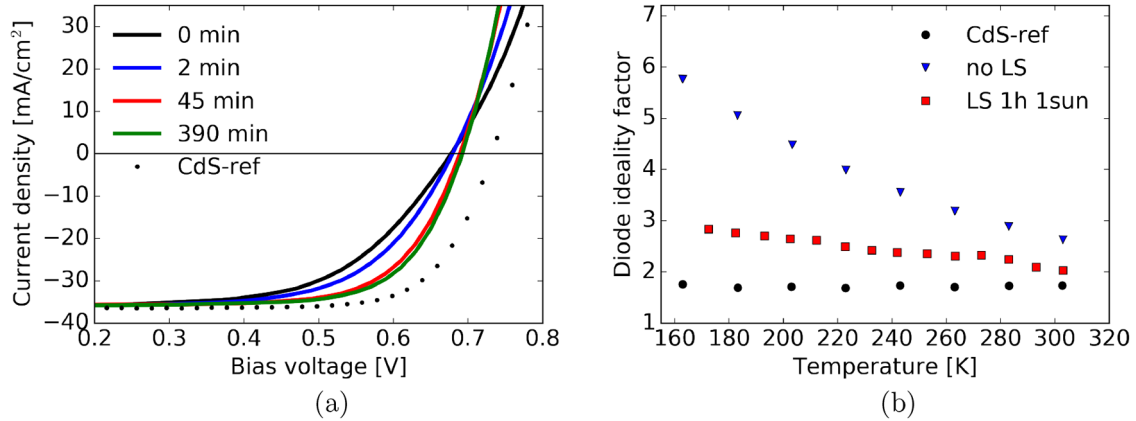


Fig. 4. (a) IV of $\text{Zn}_{1-x}\text{Mg}_x\text{O}$ buffer device before and after different light soaking duration at 1 sun. (b) Ideality factor extracted from $J_{\text{SC}}-V_{\text{OC}}$ measurements for CdS reference (circle) and $\text{Zn}_{1-x}\text{Mg}_x\text{O}$ buffer device before (triangle) and after light soaking (square).

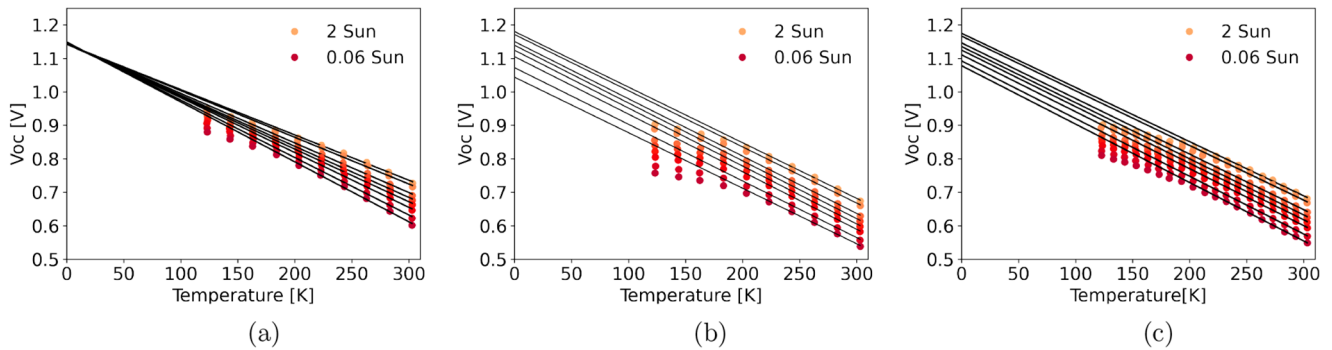


Fig. 5. Extrapolation of V_{OC} at 0 K for (a) CdS reference, (b) $\text{Zn}_{1-x}\text{Mg}_x\text{O}$ buffer (c) $\text{Zn}_{1-x}\text{Mg}_x\text{O}$ buffer after light soaking for 1 h at 1 sun.

analysed before and after light soaking at 1 sun for 1 h. The respective diode quality factor A is presented in Figure 4b, the extrapolation of V_{OC} at 0 K is presented in Figure 5. For the reference device, the ideality factor A is about 1.7 and almost insensitive to temperature. A pronounced difference before and after light soaking of the $\text{Zn}_{1-x}\text{Mg}_x\text{O}$ buffer device is visible in the respective diode ideality factors A . The relaxed $\text{Zn}_{1-x}\text{Mg}_x\text{O}$ buffer device shows A increase from 3.0 to 5.9 with decreasing temperature. After exposure to 1 sun, the ideality factor is still higher than 2, but the range has been limited to 2.1–2.9. The temperature dependence of the ideality factor of the $\text{Zn}_{1-x}\text{Mg}_x\text{O}$ buffer devices is probably linked to fluctuations in the activation energy of the dominating recombination process [62]. The fluctuation is reduced during light soaking, which is evident from the decreased values for A , but not fully eliminated.

The V_{OC} at 0 K before and after light soaking is extrapolated for the temperatures from 200 to 300 K. The reference device shows an extrapolated V_{OC} at 0 K between 1.14 and 1.15 eV, in good agreement with the bandgap of 1.14 eV extracted from the EQE curve using the Tauc fit method (Fig. 2). The device with $\text{Zn}_{1-x}\text{Mg}_x\text{O}$ buffer layer shows a spread in extrapolated V_{OC} at 0 K from 1.18 eV down to 1.05 eV before light soaking, and ranges from 1.18

to 1.08 eV after light soaking (1 h at 1 sun). The decreased extrapolated V_{OC} values suggest a dominant recombination path located at the absorber buffer interface [62] possibly mediated by a defect within the bandgap. Such an effect can also explain the reduced V_{OC} . Improved FF and V_{OC} due to the absence of shunts and a slight increase in device V_{OC} are consistent with the IV analysis for different light soaking durations presented in Figure 4a.

4 Conclusion

CIGS solar devices with ALD ZnMgO buffer layers were fabricated with efficiencies reaching 18% after light soaking. The conduction band alignment was investigated by systematically varying the $\text{Zn}_{1-x}\text{Mg}_x\text{O}$ stoichiometry, revealing a best alignment with $x = 0.16$ composition. The compositional range for suitable band alignment with CIGS is found more narrow than expected. The treatments performed to investigate the effect on the absorber surface were performed immediately prior to buffer deposition. Wet treatments using NH_4OH , thiourea or both resulted in improvements of V_{OC} and FF. Additional improvements were achieved by a single TMA pulse in vacuum, before the $\text{Zn}_{1-x}\text{Mg}_x\text{O}$ buffer deposition, which we assign to reduction

of surface species and subsequent chemical surface passivation. The best results were achieved by a combination of wet etching in KCN and NH_4OH before exposure with TMA under vacuum. The $\text{Zn}_{1-x}\text{Mg}_x\text{O}$ devices exhibit a reversible metastable light soaking effect, improving the device efficiency. Temperature and illumination dependant electrical characterization revealed increased interface recombination in $\text{Zn}_{1-x}\text{Mg}_x\text{O}$ buffer devices, as compared to the CdS reference. We consider $\text{Zn}_{1-x}\text{Mg}_x\text{O}$ as a possible alternative buffer layer for CIGS solar cells, although further work is necessary to understand and overcome the unwanted recombination mechanisms and improve cell efficiencies.

This work was partially supported by the Swiss Federal Office of Energy (contract Nr SI/501614-01 ImproCIS) and from the Swiss State Secretary for Education, Research and Innovation (SERI) under contract number 17.00105 (EMPIR project HyMet). The EMPIR programme is co-financed by the participating states and by the European Union's Horizon 2020 research and innovation programme under the Marie Skłodowska-Curie grant agreement number 754364.

Author contribution statement

R.H. conceived the idea, which was co-developed with R.C., M.O. and A.N.T. S.N. deposited the absorbers. R.H. performed device fabrication after absorber deposition, characterization of thin films and devices. E.G. conducted the XPS measurements and analysis. All authors were involved in the interpretation of the data. R.H. wrote the manuscript. All authors provided feedback and corrections to the manuscript.

References

- M. Nakamura, K. Yamaguchi, Y. Kimoto, Y. Yasaki, T. Kato, H. Sugimoto, *IEEE J. Photovolt.* **9**, 1863 (2019)
- A. Chirilă, P. Reinhard, F. Pianezzi, P. Bloesch, A.R. Uhl, C. Fella, L. Kranz, D. Keller, C. Gretener, H. Hagendorfer et al., *Nat. Mater.* **12**, 1107 (2013)
- P. Jackson, R. Wuerz, D. Hariskos, E. Lotter, W. Witte, M. Powalla, *Phys. Status Solidi (RRL) – Rapid Res. Lett.* **10**, 583 (2016)
- T. Kato, J.L. Wu, Y. Hirai, H. Sugimoto, V. Bermudez, *IEEE J. Photovolt.* **9**, 325 (2019)
- J. Lindahl, J. Keller, O. Donzel-Gargand, P. Szaniawski, M. Edoff, T. Törndahl, *Sol. Energy Mater. Sol. Cells* **144**, 684 (2016)
- F. Larsson, O. Donzel-Gargand, J. Keller, M. Edoff, T. Törndahl, *Sol. Energy Mater. Sol. Cells* **183**, 8 (2018)
- J. Löckinger, S. Nishiwaki, C. Andres, R. Erni, M.D. Rossell, Y.E. Romanyuk, S. Buecheler, A.N. Tiwari, *ACS Appl. Mater. Interfaces* **10**, 43603 (2018)
- S. Prabhar, M. Dhanam, *J. Cryst. Growth* **285**, 41 (2005)
- F. Pianezzi, P. Reinhard, A. Chirilă, B. Bissig, S. Nishiwaki, S. Buecheler, A.N. Tiwari, *Phys. Chem. Chem. Phys.* **16**, 8843 (2014)
- O. Donzel-Gargand, F. Larsson, T. Törndahl, L. Stolt, M. Edoff, *Prog. Photovolt. Res. Appl.* **27**, 220 (2019)
- H. Simchi, B.E. McCandless, K. Kim, J.H. Boyle, R.W. Birkmire, W.N. Shafarman, *IEEE J. Photovolt.* **2**, 519 (2012)
- N.H. Valdes, K.J. Jones, R.L. Opila, W.N. Shafarman, *IEEE J. Photovolt.* **9**, 1846 (2019)
- D. Hariskos, S. Spiering, M. Powalla, *Thin Solid Films* **480–481**, 99 (2005)
- S. Siebentritt, *Solar Energy* **77**, 767 (2004)
- N. Naghavi, D. Abou-Ras, N. Allsop, N. Barreau, S. Bücheler, A. Ennaoui, C.H. Fischer, C. Guillen, D. Hariskos, J. Herrero et al., *Prog. Photovolt. Res. Appl.* **18**, 411 (2010)
- J. Chantana, Y. Kawano, T. Nishimura, Y. Kimoto, T. Kato, H. Sugimoto, T. Minemoto, *Prog. Photovolt. Res. Appl.*, pip. **28**, 79 (2020)
- J. Chantana, Y. Kawano, T. Nishimura, Y. Kimoto, T. Kato, H. Sugimoto, T. Minemoto, *ACS Appl. Energy Mater.* **3**, 1292 (2020)
- O. Taurian, M. Springborg, N. Christensen, *Solid State Commun.* **55**, 351 (1985)
- Ü. Özgür, Y.I. Alivov, C. Liu, A. Teke, M. Reshchikov, S. Dogan, V. Avrutin, S.J. Cho, H. Morkoç, *J. Appl. Phys.* **98**, 11 (2005)
- C. Kılıç, A. Zunger, *Appl. Phys. Lett.* **81**, 73 (2002)
- A. Klein, *J. Phys.: Condens. Matter* **27**, 134201 (2015)
- T. Minemoto, Y. Hashimoto, T. Satoh, T. Negami, H. Takakura, Y. Hamakawa, *J. Appl. Phys.* **89**, 8327 (2001)
- M. Murata, J. Chantana, N. Ashida, D. Hironiwa, T. Minemoto, *Japanese J. Appl. Phys.* **54**, 032301 (2015)
- Y. Kuwahata, T. Minemoto, *Renew. Energy* **65**, 113 (2014)
- T. Törndahl, C. Platzer-Björkman, J. Kessler, M. Edoff, *Prog. Photovolt. Res. Appl.* **15**, 225 (2006)
- C.-S. Lee, S. Kim, E.A. Al-Ammar, H. Kwon, B.T. Ahn, *ECS J. Solid State Sci. Technol.* **3**, Q99 (2014)
- J. Pettersson, C. Platzer-Björkman, M. Edoff, *Prog. Photovolt. Res. Appl.* **17**, 460 (2009)
- S. Kim, C.S. Lee, S. Kim, R. Chalapathy, E.A. Al-Ammar, B. T. Ahn, *Phys. Chem. Chem. Phys.* **17**, 19222 (2015)
- T. Minemoto, J. Julayhi, *Curr. Appl. Phys.* **13**, 103 (2013)
- M. Sugiyama, H. Sakakura, S.W. Chang, *Electrochim. Acta* **131**, 236 (2014)
- J. Chantana, T. Kato, H. Sugimoto, T. Minemoto, *Prog. Photovolt. Res. Appl.* **26**, 127 (2018)
- J. Löckinger, S. Nishiwaki, T.P. Weiss, B. Bissig, Y.E. Romanyuk, S. Buecheler, A.N. Tiwari, *Sol. Energy Mater. Sol. Cells* **174**, 379 (2017)
- J. Serhan, Z. Djebbour, W. Favre, A. Migan-Dubois, A. Darga, D. Mencaraglia, N. Naghavi, G. Renou, J.F. Guillemoles, D. Lincot, *Thin Solid Films* **519**, 7606 (2011)
- N. Naghavi, S. Temgoua, T. Hildebrandt, J.F. Guillemoles, D. Lincot, *Prog. Photovolt. Res. Appl.* **23**, 1820 (2015)
- T. Lavrenko, T. Walter, B. Plesz, *Phys. Status Solidi C* **14**, 1600197 (2017)
- I. Repins, S. Glynn, T.J. Silverman, R. Garris, K. Bowers, B. Stevens, L. Mansfield, *Prog. Photovolt. Res. Appl.* **27**, 749 (2019)
- J. Serhan, Z. Djebbour, A. Darga, D. Mencaraglia, N. Naghavi, G. Renou, D. Lincot, J.F. Guillemoles, *Sol. Energy Mater. Sol. Cells* **94**, 1884 (2010)
- N. Naghavi, G. Renou, V. Bockelee, F. Donsanti, P. Genevee, M. Jubault, J. Guillemoles, D. Lincot, *Thin Solid Films* **519**, 7600 (2011)
- S. Lany, A. Zunger, *J. Appl. Phys.* **100**, 113725 (2006)

40. S. Lany, A. Zunger, Phys. Rev. Lett. **100**, 016401 (2008)
41. W.S. Choi, J.G. Yoon, Solid State Commun. **152**, 345 (2012)
42. F. Troni, G. Sozzi, R. Menozzi, A numerical study of the design of ZnMgO window layer for Cadmium-free thin-film CIGS solar cells, in *2011 7th Conference on Ph. D. Research in Microelectronics and Electronics* (IEEE, 2011), pp. 193–196
43. R. Carron, S. Nishiwaki, T. Feurer, R. Hertwig, E. Avancini, J. Löckinger, S.C. Yang, S. Buecheler, A.N. Tiwari, Adv. Energy Mater. **9**, 1900408 (2019)
44. B. Bissig, R. Carron, L. Greuter, S. Nishiwaki, E. Avancini, C. Andres, T. Feurer, S. Buecheler, A.N. Tiwari, Prog. Photovolt. Res. Appl. **26**, 894 (2018)
45. T. Minemoto, T. Matsui, H. Takakura, Y. Hamakawa, T. Negami, Y. Hashimoto, T. Uenoyama, M. Kitagawa, Sol. Energy Mater. Sol. Cells **67**, 83 (2001)
46. C.S. Lee, Y.M. Shin, B.T. Ahn, ECS Trans. **41**, 213 (2011)
47. E. Avancini, R. Carron, T.P. Weiss, C. Andres, M. Bürki, C. Schreiner, R. Figi, Y.E. Romanyuk, S. Buecheler, A.N. Tiwari, Chem. Mater. **29**, 9695 (2017)
48. T. Nakada, A. Kunioka, Appl. Phys. Lett. **74**, 2444 (1999)
49. T.M. Friedlmeier, P. Jackson, D. Kreikemeyer-Lorenzo, D. Hauschild, O. Kiowski, D. Hariskos, L. Weinhardt, C. Heske, M. Powalla, A closer look at initial CdS growth on high-efficiency Cu(In,Ga)Se₂ absorbers using surface-sensitive methods, in *2016 IEEE 43rd Photovoltaic Specialists Conference (PVSC)*, (IEEE, 2016), pp. 0457–0461
50. C. Platzer-Björkman, T. Törndahl, A. Hultqvist, J. Kessler, M. Edoff, Thin Solid Films **515**, 6024 (2007)
51. F. Larsson, L. Stolt, A. Hultqvist, M. Edoff, J. Keller, T. Törndahl, ACS Appl. Energy Mater. **3**, 7208 (2020)
52. T. Nakada, H. Ohbo, T. Watanabe, H. Nakazawa, M. Matsui, A. Kunioka, Sol. Energy Mater. Sol. Cells **49**, 285 (1997)
53. K. Nakada, M. Watanabe, T. Nishimura, N. Suyama, A. Yamada, Japanese J. Appl. Phys. **59**, 031005 (2020)
54. W. Witte, D. Hariskos, M. Powalla, Thin Solid Films **519**, 7549 (2011)
55. J. Keller, F. Gustavsson, L. Stolt, M. Edoff, T. Törndahl, Sol. Energy Mater. Sol. Cells **159**, 189 (2017)
56. P. Alen, M. Juppó, M. Ritala, T. Sajavaara, J. Keinonen, M. Leskelä, J. Electrochem. Soc. **148**, G566 (2001)
57. K. Koike, K. Hama, I. Nakashima, S. Sasa, M. Inoue, M. Yano, Japanese J. Appl. Phys. **44**, 3822 (2005)
58. G. Luka, L. Wachnicki, B.S. Witkowski, T.A. Krajewski, R. Jakiela, E. Guziewicz, M. Godlewski, Mater. Sci. Eng. B **176**, 237 (2011)
59. Y. Inoue, M. Hala, A. Steigert, R. Klenk, S. Siebentritt, Optimization of buffer layer/i-layer band alignment, in *2015 IEEE 42nd Photovoltaic Specialist Conference, PVSC 2015* Institute of Electrical and Electronics Engineers Inc. (2015)
60. W. Metzger, I. Repins, M. Romero, P. Dippo, M. Contreras, R. Noufi, D. Levi, Thin Solid Films **517**, 2360 (2009)
61. Y. Ando, S. Ishizuka, S. Wang, J. Chen, M.M. Islam, H. Shibata, K. Akimoto, T. Sakurai, Jpn. J. Appl. Phys. **57**, 08RC08 (2018)
62. R. Scheer, H.W. Schock, *Chalcogenide photovoltaics: physics, technologies, and thin film devices*, (John Wiley & Sons, Weinheim, 2011)

Cite this article as: Ramis Hertwig, Shiro Nishiwaki, Mario Ochoa, Shih-Chi Yang, Thomas Feurer, Evgeniia Gilshtein, Ayodhya N. Tiwari, Romain Carron, ALD-ZnMgO and absorber surface modifications to substitute CdS buffer layers in co-evaporated CIGSe solar cells, EPJ Photovoltaics 11, 12 (2020)